frontiers | Frontiers in Earth Science

TYPE Original Research
PUBLISHED 04 January 2023
DOI 10.3389/feart.2022.1031842

OPEN ACCESS

EDITED BY
Fan Yang,
Lanzhou University, China

REVIEWED BY
Yinhang Cheng,
China Geological Survey, China
Leilei Dong,
University of Science and Technology Beijing, China

*CORRESPONDENCE
Yingjie Li,
liyingjie820@126.com

SPECIALTY SECTION
This article was submitted to Structural Geology and Tectonics, a section of the journal Frontiers in Earth Science

RECEIVED 30 August 2022
ACCEPTED 12 December 2022
PUBLISHED 04 January 2023

CITATION
Zhang X, Li Y, Wang G, Wang S, Kong X, Wang X and Liu Z (2023), Intra-oceanic subduction in the southeastern Paleo-Asian ocean: Evidence from early Permian gabbro of the Diyanmiao ophiolite in central Inner Mongolia, North China.
Front. Earth Sci. 10:1031842.
doi: 10.3389/feart.2022.1031842

Intra-oceanic subduction in the southeastern Paleo-Asian ocean: Evidence from early Permian gabbro of the Diyanmiao ophiolite in central Inner Mongolia, North China

Xiawei Zhang[1,2], Yingjie Li[2,3]*, Genhou Wang[1], Shuai Wang[1,2], Xingrui Kong[3], Xiaodong Wang[3] and Zhibin Liu[3]

[1]School of the Earth Sciences and Resources, China University of Geosciences, Beijing, China, [2]Hebei Key Laboratory of Strategic Critical Mineral Resources, Heibei GEO University, Shijiazhuang, China, [3]College of Earth Sciences, Hebei GEO University, Shijiazhuang, China, [4]Hebei Province Collaborative Innovation Center for Strategic Critical Mineral Research, Hebei GEO University, Shijiazhuang, China

Investigation of intra-oceanic subduction can improve our understanding of plate tectonic processes and the history of continental growth. Evidence for intra-oceanic subduction in the Paleo-Asian Ocean has recently become an important focus of research, including the Diyanmiao ophiolite in central Inner Mongolia, North China. Here, we report a newly discovered occurrence of early Permian gabbro in the Diyanmiao ophiolite zone. The gabbro yields a weighted mean zircon U–Pb age of 294.4 ± 2.2 Ma. The gabbro samples are characterized by moderate SiO_2 (47.32–50.51 wt%), low TiO_2 (0.26–0.54 wt %) and K_2O (0.04–0.75 wt%), and high Na_2O (1.84–4.52 wt%) contents, high Na_2O/K_2O ratios (2.92–58.29), and depleted chondrite-normalized light rare Earth element patterns that are similar to N-MORB. The gabbros show slightly lower contents of high-field-strength elements (e.g., Nb, Ta, and Ti) and slightly higher contents of large-ion lithophile elements (e.g., K, Rb, Ba, and U) relative to N-MORB. In addition, the gabbros show high ε_{Nd} (t) values (8.0–9.8) that are similar to those of forearc basalt in the Diyanmiao ophiolite and N-MORB. Integrating these new data with available results for ophiolite and arc-magmatic rocks of central Inner Mongolia, we propose that the studied gabbro was formed during the initial stage of intra-oceanic subduction and that the Paleo-Asian Ocean was still in a subduction setting during the early Permian.

KEYWORDS

geochronology, gabbro, early permian, intra-oceanic subduction, Paleo-Asian Ocean

1 Introduction

Ophiolites represent fragments of ancient oceanic lithosphere in continental orogenic belts and record the magmatic evolution, metamorphic history, and structural processes of oceanic lithosphere, and also provide important information on the development and extinction of ancient oceanic basins (Nicolas, 1989). Ophiolites form in a variety of plate tectonic settings (e.g., Nicolas, 1989; Dilek and Robinson, 2003; Dilek and Furnes, 2009, 2011, 2014; Kusky, 2011; Santosh et al., 2016) and are eventually obducted onto continental margins or incorporated into accretionary prisms and orogens, thereby serving as marker zones of accretion and suturing between crustal blocks that were originally separated by oceanic basins (Dilek and Furnes, 2011). Consequently, the geology, geochemistry, and geochronology of ophiolites and spatially associated lithological units provide important insights into the evolution of major orogenic belts (Shervais et al., 2004).

The Central Asian Orogenic Belt (CAOB) was formed during a prolonged process involving subduction, accretion, and collision of the Paleo-Asian oceanic plate (Dobretsov et al., 1995). This belt was subsequently superimposed and transformed by the Mesozoic Mongolia–Okhotsk and Pacific tectonic regimes. The CAOB is considered the world's largest Phanerozoic accretionary orogen and is located between the Siberian Craton to the north and the Tarim and North China cratons to the south (Figure 1A). The belt contains intra-oceanic forearc materials, oceanic islands and seamounts, and ancient oceanic crust fragments as a result of the subduction of the Paleo-Asian oceanic plate (Badarch et al., 2002; Windley et al., 2007; Xiao et al., 2009, 2014; Kröner et al., 2017; Safonova, 2017; Yang et al., 2017, 2021; Cheng et al., 2019; Ma et al., 2021).

The southeastern part of the CAOB is a key area for exploring the Paleozoic tectonic evolution of this orogenic belt, as it contains numerous ophiolite belts, including the Erenhot–Hegenshan ophiolite belt (EHOB), Linxi belt, and Xar Moron River belt (XMRB), which are thought to mark the location of final closure of the Paleo-Asian Ocean (PAO) (Wang and Liu, 1986; Tang, 1990; BGMRIMAR, 1996; Xiao et al., 2003; Song et al., 2015; Yuri et al., 2020) (Figures 1B, C). Although the EHOB is traditionally considered to have formed in a mid-ocean ridge basalts (MORB) (Nozaka and Liu, 2002), the formation of most Inner Mongolia ophiolites is ascribed to a supra-subduction zone (SSZ) environment on the basis of the geochemistry of their magmatic rocks (e.g., Shervais, 2001). Such ophiolites include the Neo-Tethyan ophiolite in SW Turkey (Aldanmaz et al., 2009) and the Troodos ophiolite in Cyprus (Osozawa et al., 2012).

Two models have been proposed for the late Paleozoic evolution of the PAO. Some studies have suggested that continuous subduction of the Paleo-Asian oceanic plate induced multiple accretion events on the Uliastai continental margin (UCM) and the northern margin of the Sino-Korean paleoplate during the Paleozoic. The collision of two paleoplates along the Solonker–Linxi or Xar Moron River belts led to the final formation of the CAOB during the late Permian or Early Triassic (Windley, 1993; Xiao et al., 2003; Cheng et al., 2014, 2015). Other studies have argued that the PAO closed during the early or middle Paleozoic along the EHB or the Xilin Hot–Heihe suture zone and that the Carboniferous and Permian ophiolites in the area formed in a rift setting (Xu et al., 2013; Zhao et al., 2015). The main difference between the two models is whether the southeastern PAO was in a subduction or extensional tectonic setting during the late Paleozoic.

During recent work, we identified early Permian gabbro fragments in the Diyanmiao ophiolitic mélange of southeastern Inner Mongolia. These fragments represent northward subduction of the Paleo-Asian oceanic plate beneath the southern margin of the Siberian plate and formed after the early Carboniferous–early Permian (Li et al., 2018) (Figure 2). In this paper, we combine new data on the petrology, geochronology, and geochemistry of gabbro from the Diyanmiao ophiolite with results of previous studies in this area to establish the evolution of the PAO during the late Carboniferous and early Permian.

2 Geological setting

Five NEE–SWW-trending tectonic zones have been identified in southeastern Inner Mongolia: the Southern orogenic belt, the Solonker suture zone, the Northern orogenic belt (NOB), the EHOB, and the UCM from south to north (Figure 1B) (Xiao et al., 2003; Jian et al., 2012).

The UCM contains post-collisional basalts, andesites, and pyroclastic deposits of late Carboniferous–Permian age. These volcanic–sedimentary sequences overlie Cambrian to Devonian shallow-marine and continental fine clastic rocks (Zhang et al., 2011; Li et al., 2014; Anas et al., 2020). The EHOB lies to the south of the UCM and is characterized by numerous ophiolite slices, including the Hegenshan, Baiyinbulage, and Diyanmiao ophiolites from west to east (Li et al., 2015), which are enclosed in Carboniferous–Permian flysch (Wang and Liu, 1986; Liang, 1991). The EHOB extends from Erenhot, close to the China–Mongolia border, in the southwest to Hegenshan in the northeast. The EHOB is separated from the NOB to the south by the Solonker suture zone (Figure 1B). The NOB comprises the Xilin Gol and Baolidao Arc complexes (Xiao et al., 2003). The Xilin Gol complex, which is thought to represent Precambrian basement (e.g., Ge et al., 2011; Sun et al., 2013), consists mainly of biotite and muscovite schists, quartz–feldspar gneisses, and plagioclase amphibolites (Xiao et al., 2003; Chen et al., 2009). This complex is unconformably overlain by a cover of late Carboniferous

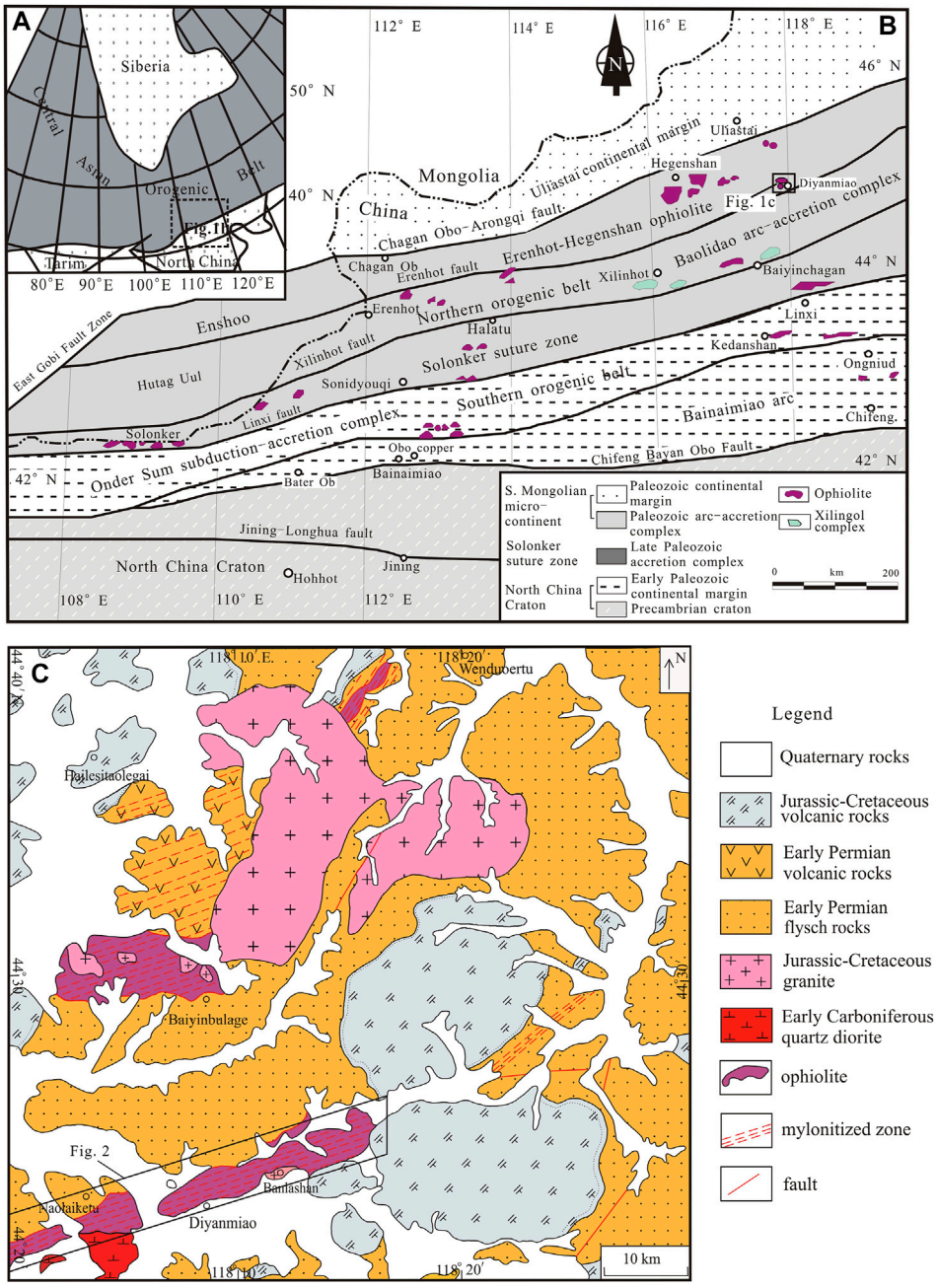

FIGURE 1
(A) Schematic tectonic division of north China-Mongolia segment (modified from Jahn, 2004). **(B)** Sketch geological map of the late Paleozoic crust of southeastern Inner Mongolia (modified from Xiao et al., 2003). **(C)** Simplified geological map of the Diyanmiao area (modified after Li et al., 2020a).

and Permian marine strata (Li et al., 2018). The Baolidao Arc complex, which extends from Bayanbaolidao to Xilinhot, is composed of cumulate gabbros, gabbro diorites, quartz diorites, tonalites, and granites, and represents a magmatic arc formed by northward seafloor subduction (Xiao et al., 2003, 2009; Jian et al., 2008).

3 Field and petrographic features

The Diyanmiao ophiolite is located in West Ujimqin, eastern Inner Mongolia (Figure 1B), and is divided into the Naolaiketu ophiolite to the south and the Baiyinbulage ophiolite to the north (Li et al., 2018; 2020a). The

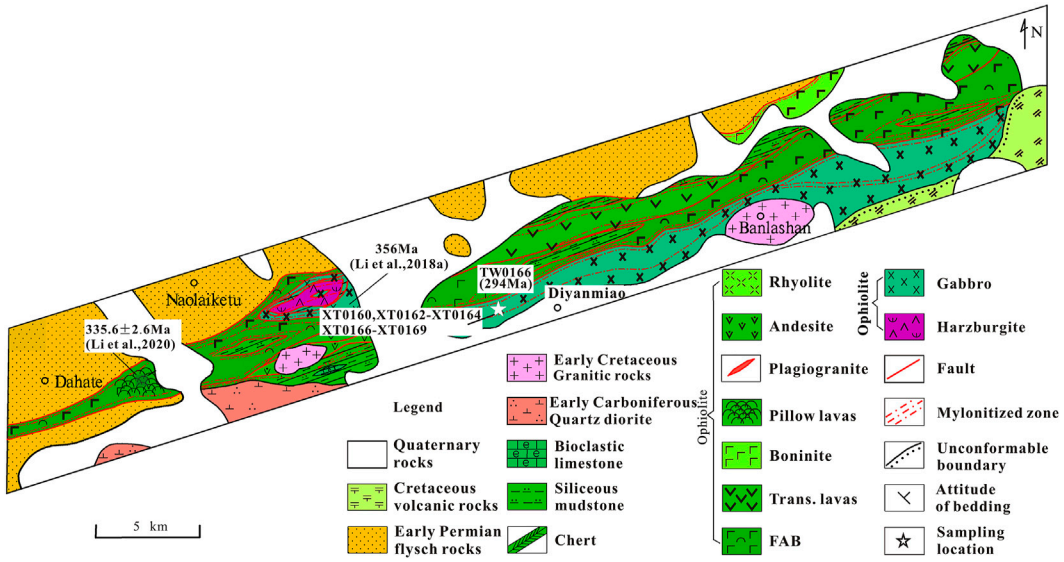

FIGURE 2
Simplified geological map of the Naolaiketu ophiolite in Diyanmiao (modified after Li et al., 2020a).

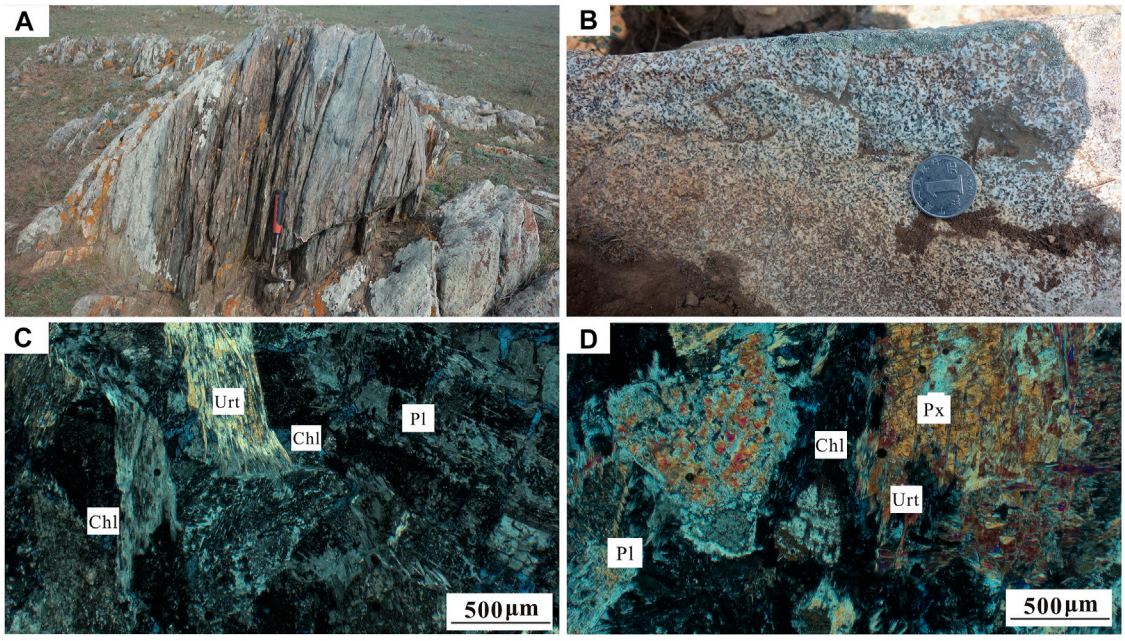

FIGURE 3
Macrofeatures and photomicrographs of the gabbro in Diyanmiao ophiolite. **(A)**-outcrop of gabbro; **(B)**-hand specimen of gabbro; **(C,D)**-photomicrographs of gabbro; Pl, plagioclase; Px, pyroxene; Chl, chlorite; Urt, uralite.

Naolaiketu ophiolite is exposed in the Naolaiketu–Diyanmiao area as an ENE–WSW-trending belt with a width of ~3 km and length of ~28 km. In the ophiolite belt, well-developed ductile deformation is shown by the development of folds, ENE–WSW-trending stretching lineations, and mylonitic microstructures, as well as domains with strongly developed rhombic-meshed structure and weakly deformed domains. The lithological units comprise serpentinized

harzburgite, layered gabbro, fine-grained isotropic gabbro, spilite, basalt, and quartz keratophyres, from bottom to top, and are overlain by chert. Of these, spillite and fine-grained isotropic gabbro are the most widely exposed. At the site of fault contact of the ophiolite and early Permian strata (Shoushangou and Dashizhai formations), well-developed brittle deformation structures are observed, including cleavages and cataclasite bands. Compressed and fragmented belts of ophiolite range in width from several meters to hundreds of meters.

For this study, samples of fine-grained isotropic gabbro (Figure 2) were obtained for geochemical and geochronological analyses (Figures 3A, B). The gabbro mainly consists of fine-grained, tabular plagioclase (40–45 vol%) and granular pyroxene (35–40 vol%), with minor magnetite and ilmenite (~5 vol%). The rock shows hypidiomorphic and granular textures under the microscope (Figures 3C, D). The rocks have been strongly altered, including replacement of plagioclase by zoisite and pyroxene by uralite.

4 Analytical techniques

4.1 *In situ* zircon U–Pb dating

One sample of gabbro (TW0166) was selected for *in situ* zircon U–Pb dating. Zircon grains were separated by crushing, sieving, and standard heavy-liquid techniques, followed by hand-picking under a binocular microscope at the Laboratory of Regional Geology and Mineral Resources Research Institute of Hebei Province, Langfang, China. The separated zircons were mounted in epoxy resin discs and polished to expose the grain interiors for analyses. Transmitted- and reflected-light photomicrographs, as well as cathodoluminescence (CL) images, were obtained to reveal zircon internal structure. CL images were acquired using a scanning electron microscope (JSM6510) equipped with a GATAN CL instrument at Beijing Gaonianlinghang Geo Analysis, Beijing, China.

Zircon U–Pb dating was performed using laser-ablation–multi-collector–inductively coupled plasma–mass spectrometry (LA–MC–ICP–MS) at the Tianjin Institute of Geology and Mineral Resources, China. The instrumental conditions and analytical processes were similar to those described by Liu et al. (2008). Operating conditions included a laser spot diameter of 32 μm and a laser frequency of 7 Hz. Contents of U and Pb were calibrated by using the standard zircon TEMORA (417 Ma), while zircon GJ-1 (597 Ma) was used as the external standard. The Excel-based software ICPMSDataCal program (Liu et al., 2008) was used to calculate U and Th contents and U–Pb dating results, including calibrations, and the ISOPLOT 4.15 program (Ludwig, 2003) was used to plot results.

4.2 Whole-rock major and trace element analyses

We selected eight representative samples of the gabbro for bulk-rock major- and trace-element analyses at the Tianjin Geological Survey Center of China Geological Survey, China. Major elements were analyzed using X-ray fluorescence (XRF) spectrometry (Rigaku 3270E) with high-dispersion Echelle optics. Analyses of Chinese national standard rock samples GSR-1, GSR-2, and GSR-3 revealed that the analytical precision is generally better than ±2% for most major elements.

Bulk-rock trace-element analyses were performed using ICP–MS at the Tianjin Geological Survey Center of China Geological Survey following the analytical procedure of Liu et al. (2008). The analytical precision for most trace elements is better than 5%, as monitored by analyses of Chinese national standard samples GSR-1 and GSR-3. The analytical precision was better than ±5% for trace elements.

4.3 Sr and Nd isotopes

Sr and Nd isotope ratios were measured for 12 samples using a Thermo-Finnigan VG Sector 54 thermal ionization mass spectrometer at the Tianjin Geological Survey Center of China Geological Survey following the analytical procedures described by Miao et al. (2008). Ratios of $^{87}Rb/^{86}Sr$ and $^{147}Sm/^{144}Nd$ were calculated using the Rb, Sr, Sm, and Nd contents determined by ICP–MS. The mass fractionation corrections for isotopic ratios were measured using a value of 0.1194 for $^{86}Sr/^{88}Sr$ and 0.7219 for $^{146}Nd/^{144}Nd$. The USGS rock standard BCR-2 was used to evaluate the separation and purification process of Rb, Sr, Sm, and Nd, yielding $^{87}Sr/^{86}Sr = 0.704963 \pm 0.000003$ and $^{143}Nd/^{144}Nd = 0.512354 \pm 0.000004$.

5 Analytical results

5.1 Zircon U–Pb geochronology

Zircon CL images from the fine-grained isotropic gabbro sample TW0166 are shown in Figure 4, and zircon U–Pb isotope data are given in Table 1. Most of the zircons are clear, euhedral, and short or granular prismatic crystals with lengths of 50–100 μm and aspect ratios of 1:1 to 2:1. The grains show well-developed straight and wide oscillatory zoning in CL images, consistent with mafic volcanic or gabbroic rocks (Song et al., 2015).

Fifteen spots were analyzed on 15 zircon grains from sample TW0166. Contents of Th and U and Th/U ratios of the zircons are 14–354 ppm, 40–399 ppm, and 0.73–4.67, respectively. All ages show concordance on a $^{206}Pb/^{238}U$–$^{207}Pb/^{235}U$ concordia diagram (Figure 4). The analytical result yield a weighted

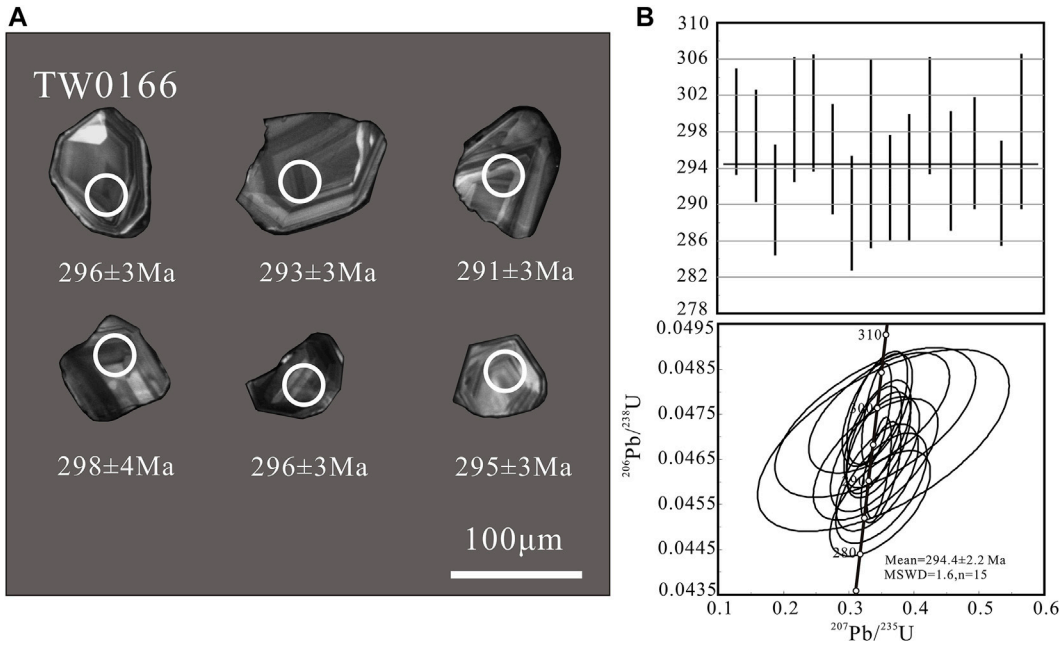

FIGURE 4
(A) Representative cathodoluminescence (CL) images of zircons from gabbro sample TW0166 **(B)** Zircon U-Pb concordia diagrams and weighed mean age for the gabbro sample TW0166.

mean $^{206}Pb/^{238}U$ age of 294.4 ± 2.2 Ma (MSWD = 1.6, 2σ), which is interpreted as the crystallization age of the gabbro.

5.2 Major and trace element compositions

The Diyanmiao gabbro samples have SiO_2 = 46.94–50.51 wt% (mean = 48.62 wt%) and MgO = 7.56–10.02 wt% (mean = 8.88 wt%), with $Mg^{\#}$ values of 65.0–75.6 (mean = 70.3). The samples are characterized by high contents of Al_2O_3 (14.26–17.53 wt%) and CaO (9.92–14.61 wt%), but low contents of $Fe_2O_3^T$ (as FeO + Fe_2O_3, 5.53–8.31 wt%), TiO_2 (0.26–0.54 wt%), MnO (0.12–0.17 wt%), and P_2O_5 (0.01–0.04 wt%). The gabbro samples also have low contents of total rare Earth elements (REEs) (∑REEs) (10.76–20.68 ppm, mean = 15.98 ppm) and low ratios of light REEs to heavy REEs (LREE/HREE) (0.97–1.31), $(La/Yb)_N$ (0.47–0.89), $(Gd/Yb)_N$ (0.91–1.07), $(La/Sm)_N$ (0.56–0.99), and $(Sm/Nd)_N$ (1.12–1.28). But positive Eu anomalies (Eu/Eu* = 1.12–1.53), similar to the characteristics of N-MORB, including flat REE patterns (Table 2; Figure 5A). In a primitive-mantle-normalized spider diagram (Figure 5B), the gabbros show positive Rb, K, and Sr anomalies and negative Th, Ta, Zr, and Nb anomalies. Depletion in Nb relative to La and Th indicates the involvement of continental crust or arc materials during magmatic evolution (e.g., Santosh et al., 2017).

5.3 Sr and Nd isotopic compositions

The Diyanmiao gabbros show high ε_{Nd} (t = 294.4 Ma) values (+8.0 to +9.8). The ε_{Nd} (t) values are similar to FABs of the Diyanmiao ophiolite (Table 3; Figure 6). In contrast, the gabbros have lower $^{87}Sr/^{86}Sr$ values (0.702934–0.703131) compared with the FABs (0.70466–0.70517) (Figure 6; Table 3), which might be due to alteration, given the high mobility Figure 7 of Rb and Sr.

6 Discussion

6.1 Geochronology of the gabbro in Diyanmiao ophiolite

Previous zircon U–Pb analyses of gabbro from the Diyanmiao ophiolite have yielded ages of 346 ± 2, 357 ± 4, and 340 ± 14 Ma (Song et al., 2015; Li et al., 2018), and Diyanmiao FAB has LA-ICP-MS zircon U-Pb age of 335.6 ± 2.6 Ma (Li et al., 2020a). Previous studies have reported SHRIMP U–Pb ages of 354 ± 7 Ma and 333 ± 4 Ma for microgabbro and plagiogranite from the Hegenshan ophiolite, respectively (Jian et al., 2012), 354 ± 5 Ma and 353 ± 4 Ma for gabbro and 345 ± 6 Ma for plagiogranite from the Eastern Erenhot ophiolite (Zhang et al., 2015), and 343 ± 7 Ma for plagiogranite from the Jiaoqier ophiolite (Miao et al., 2007).

10.3389/feart.2022.1031842

TABLE 1 LA-MC-ICP-MS zircon U-Pb isotopic analysis of the gabbro in Diyanmiao ophiolite.

Spots no.	Element (ppm)		Th/U	Isotopic ratios						Apparent age (Ma)					
	Th	U		$^{206}Pb/^{238}U$	1σ	$^{207}Pb/^{235}U$	1σ	$^{207}Pb/^{206}Pb$	1σ	$^{206}Pb/^{238}U$	1σ	$^{207}Pb/^{235}U$	1σ	$^{207}Pb/^{206}Pb$	1σ
TW0166 Gabbro															
01	354	340	1.04	0.0475	0.0005	0.3425	0.0093	0.0523	0.0014	299	3	299	8	299	61
02	98	122	0.80	0.0471	0.0005	0.3439	0.0210	0.0530	0.0032	296	3	300	18	328	139
03	131	102	1.28	0.0461	0.0005	0.3434	0.0258	0.0540	0.0041	291	3	300	22	372	171
04	16	74	0.22	0.0475	0.0005	0.3465	0.0442	0.0529	0.0069	299	3	302	38	323	294
05	65	138	0.47	0.0476	0.0005	0.3435	0.0190	0.0523	0.0029	300	3	300	17	298	125
06	83	159	0.52	0.0468	0.0005	0.3455	0.0201	0.0535	0.0031	295	3	301	18	351	129
07	308	135	2.28	0.0459	0.0005	0.3500	0.0285	0.0553	0.0045	289	3	305	25	426	183
08	156	399	0.39	0.0463	0.0005	0.3461	0.0077	0.0542	0.0012	292	3	302	7	379	49
09	22	78	0.28	0.0465	0.0006	0.3411	0.0391	0.0532	0.0062	293	3	298	34	337	262
10	50	125	0.40	0.0476	0.0005	0.3435	0.0220	0.0523	0.0033	300	3	300	19	300	145
11	36	87	0.41	0.0466	0.0005	0.3400	0.0279	0.0529	0.0044	294	3	297	24	324	188
12	14	178	0.08	0.0469	0.0005	0.3385	0.0174	0.0523	0.0027	296	3	296	15	299	116
13	215	239	0.90	0.0455	0.0005	0.3479	0.0314	0.0554	0.0049	287	3	303	27	429	198
14	281	335	0.84	0.0462	0.0005	0.3490	0.0125	0.0548	0.0019	291	3	304	11	403	80
15	21	40	0.52	0.0473	0.0007	0.3407	0.0629	0.0522	0.0097	298	4	298	55	295	422

TABLE 2 Major (wt%), trace element (×l0^{-6}) analyzing results of the gabbro in Diyanmiao ophiolite and N-MORB.

Rock type	Gabbro								N-MORB
Sample NO.	XT0160	XT0162	XT0163	XT0164	XT0166	XT0167	XT0168	XT0169	
SiO_2	47.75	48.38	49.10	50.51	46.94	48.92	50.07	47.32	49.30
Al_2O_3	16.68	16.56	16.94	17.53	16.88	15.26	14.26	15.11	17.04
$Fe_2O_3^T$	8.74	8.00	8.04	7.27	5.86	6.99	6.67	7.23	6.82
CaO	12.11	11.03	10.14	9.92	15.70	13.47	14.50	14.61	11.70
MgO	8.24	8.04	8.23	7.56	9.19	10.02	9.92	9.86	7.19
K_2O	0.75	0.26	0.25	0.27	0.04	0.05	0.04	0.09	0.16
Na_2O	2.19	4.52	3.78	3.65	2.39	1.84	1.84	2.59	2.73
TiO_2	0.54	0.48	0.51	0.51	0.26	0.44	0.35	0.47	1.49
P_2O_5	0.04	0.03	0.03	0.03	0.02	0.02	0.01	0.03	0.16
MnO	0.15	0.13	0.14	0.12	0.12	0.16	0.17	0.17	0.17
LOI	2.75	2.44	2.78	2.57	2.58	2.57	2.12	2.49	
Na_2O/K_2O	2.92	17.38	15.12	13.52	58.29	40.00	48.42	30.47	17.06
$Mg^{\#}$	65.00	66.48	66.84	67.2	75.56	73.84	74.53	72.88	65.27
Rb	10	8	8	8	5	5	5	5	0.56
Cr	352	296	348	318	581	769	646	612	
Co	37	32.1	36.3	33	32.1	38.2	35.8	31.3	
Ni	115	125	148	136	107	96.7	103	99.9	
Sc	34.8	28	36	28.1	37	68	43.6	41.4	
V	193	138	157	143	154	238	214	208	
Zr	20.1	15.6	14.8	15.4	4.23	11.8	7.48	13.7	74
Hf	0.75	0.6	0.58	0.6	0.21	0.54	0.3	0.55	2.05
Rock type	Gabbro								N-MORB
Sample NO.	XT0160	XT0162	XT0163	XT0164	XT0166	XT0167	XT0168	XT0169	
Ta	0.04	0.04	0.04	0.04	0.03	0.03	0.03	0.03	0.13
Sr	122	138	143	152	141	117	112	127	90
Ba	45.1	68.2	74.3	94.9	41.8	58.4	43.6	43.7	6.3
Nb	1.06	0.82	0.79	0.96	0.84	1.06	1.02	0.86	2.33
Cs	0.78	0.7	0.77	0.78	0.45	0.54	0.42	0.72	0.01
Ga	15.2	13.1	14.4	14	10.9	14.2	10.2	12.4	
Pb	3.07	3.07	2.9	2.77	5.54	3.29	3.17	3.31	0.3
Th	0.05	0.04	0.04	0.03	0.03	0.10	0.14	0.06	0.12
U	0.05	0.04	0.05	0.04	0.05	0.03	0.03	0.04	0.05
Y	14.3	10.6	11.1	10.6	7.62	13.1	10.3	10.9	28
La	1.47	1.32	1.35	1.27	0.96	1.08	1.57	1.30	2.50
Ce	3.18	2.55	2.62	2.41	1.52	2.23	1.63	2.47	7.50

(Continued on following page)

TABLE 2 (*Continued*) Major (wt%), trace element ($\times 10^{-6}$) analyzing results of the gabbro in Diyanmiao ophiolite and N-MORB.

Rock type	Gabbro								N-MORB
Sample NO.	XT0160	XT0162	XT0163	XT0164	XT0166	XT0167	XT0168	XT0169	
Pr	0.67	0.55	0.57	0.52	0.33	0.48	0.5	0.47	1.32
Nd	3.80	3.07	3.15	2.91	1.82	2.89	2.58	2.73	7.30
Sm	1.46	1.15	1.15	1.07	0.73	1.21	0.99	1.07	2.63
Eu	0.75	0.54	0.6	0.57	0.43	0.56	0.49	0.49	1.02
Gd	2.05	1.54	1.7	1.6	1.01	1.89	1.44	1.54	3.68
Tb	0.38	0.3	0.31	0.3	0.2	0.36	0.29	0.3	0.67
Dy	2.53	1.96	2.08	1.93	1.39	2.42	1.98	2.03	4.55
Ho	0.56	0.42	0.46	0.43	0.31	0.53	0.42	0.44	1.01
Er	1.62	1.2	1.31	1.18	0.90	1.50	1.20	1.27	2.97
Tm	0.25	0.18	0.20	0.18	0.14	0.22	0.18	0.19	0.46
Yb	1.69	1.22	1.30	1.20	0.89	1.52	1.18	1.23	3.05
Lu	0.27	0.18	0.20	0.18	0.13	0.24	0.18	0.19	0.46
∑REE	20.68	16.18	17	15.75	10.76	17.13	14.63	15.72	39.11
LREE	11.33	9.18	9.44	8.75	5.79	8.45	7.76	8.53	22.27
HREE	9.35	7.00	7.56	7.00	4.97	8.68	6.87	7.19	16.84
LREE/HREE	1.21	1.31	1.25	1.25	1.16	0.97	1.13	1.19	1.32
$(La/Yb)_N$	0.59	0.73	0.70	0.71	0.73	0.48	0.90	0.71	0.59
δEu	1.33	1.24	1.31	1.33	1.53	1.13	1.25	1.17	1.00

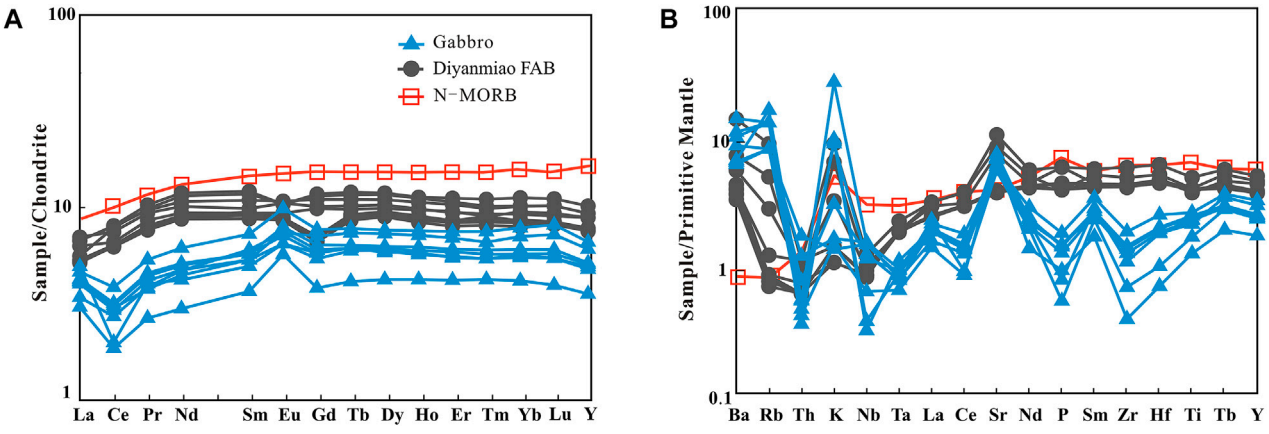

FIGURE 5
(A) Chondrite-normalized REE (Boynton, 1984)and **(B)** trace element patterns (Sun and McDonough, 1989) for the gabbro and fore-arc basalt (FAB) in the Diyanmiao ophiolite. Data of Diyanmiao FAB is after (Li et al., 2020a). N-MORB values are after Sun and McDonough, 1989.

The EHOB is considered to be a giant ophiolitic complex that developed during the Carboniferous (Wang and Liu, 1986; Tang, 1990; Song et al., 2015). Li et al. (2018) suggested that the Erenhot–Hegenshan paleo-ocean underwent intra-oceanic subduction, resulting in the formation of incipient arc crust during the early Carboniferous. The structural location

TABLE 3 Sr–Nd isotopic compositions of the gabbro in Diyanmiao ophiolite.

Sample	Age	$^{87}Rb/^{86}Sr$	$^{87}Sr/^{86}Sr$	2δ*	$(^{87}Sr/86Sr)i$	$^{147}Sm/^{144}Nd$	$^{143}Nd/^{144}Nd$	2δ	ε_{Nd} (*t*)
Gabbro									
XT0166	294	0.1026	0.703131	0.000007	0.7028	0.2425	0.513092	0.000001	8.0
XT0167	293	0.1236	0.703052	0.000009	0.7027	0.2532	0.513206	0.000001	9.8
XT0168	295	0.1291	0.702934	0.000007	0.7025	0.2320	0.513128	0.000001	9.1
XT0169	295	0.1139	0.702975	0.000008	0.7026	0.2370	0.513174	0.000001	9.8

[87]Note: (1) $(^{87}Sr/^{86}Sr)_i = Sr/^{86}Sr - ^{87}Rb/^{86}Sr \times (e^{\lambda T}-1)$, where $\lambda_{Rb} = 1.42 \times 10^{-11} year^{-1}$. (2) $\varepsilon_{Nd}(t) = \{[^{143}Nd/^{144}Nd - ^{147}Sm/^{144}Nd \times (e^{\lambda T}-1)]/[^{143}Nd/^{144}Nd]_{CHUR(0)} - (^{147}Sm/^{144}Nd)_{CHUR(0)} \times (e^{\lambda T}-1) - 1\} \times 10{,}000$, where $\lambda_{Sm} = 6.54 \times 10^{-12} year^{-1}$; $(^{143}Nd/^{144}Nd)_{CHUR(0)} = 0.512638$; $(^{147}Sm/^{144}Nd)_{CHUR(0)} = 0.1967$.

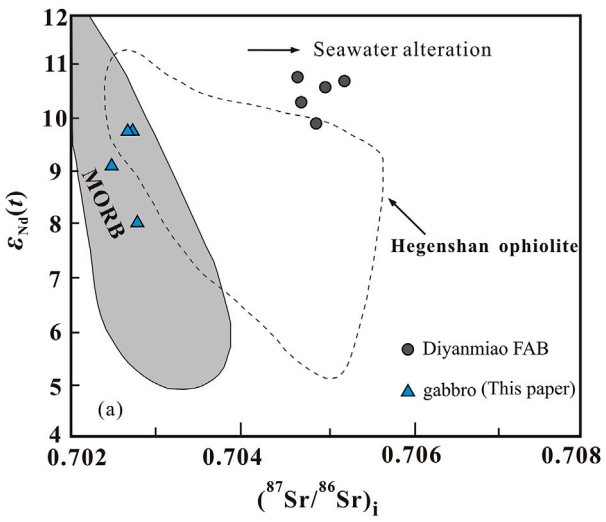

FIGURE 6
Isotopic plot of whole-rock ε_{Nd} (*t*) vs. $(^{87}Sr/^{86}Sr)_i$ for the gabbro in the Diyanmiao ophiolite; Data sources: Miao et al. (2008) for the field of Hegenshan ophiolite; Li et al. (2020a) for Diyanmiao FAB.

between the early Permian Shoushangou and Dashizhai formations indicates that the tectonic emplacement of the Diyanmiao ophiolite occurred after the early Permian.

The new LA–MC–ICP–MS zircon U–Pb age of 294.4 ± 2.2 Ma obtained from the Diyanmiao gabbro in this study gives an early Permian age for the Diyanmiao ophiolite. The age distribution of magmatic rocks of the Diyanmiao ophiolitic mélange indicates that the mélange includes rocks corresponding to at least two magmatic events, which provides important evidence regarding the timing of closure of the PAO.

6.2 Petrogenesis of the gabbro in Diyanmiao ophiolite

The studied gabbro samples show high LOI values (2.12–2.78 wt%), indicating variable alteration (Li et al., 2018), and some of the major elements (e.g., Si, Ca, K, and Ba) and trace elements (Cs and Rb) may have been mobilized to variable extents during post-magmatic hydrothermal alteration or metamorphism (Gillis and Banerjee, 2000). In contrast, some transition elements (e.g., Cr, Ti, Ni, and V), Th, high-field-strength elements (HFSEs), and REEs (Pearce, 1983) are considered to be relatively immobile during hydrothermal seafloor alteration and low-grade metamorphism (Pearce, 2008). Consequently, the following discussion of petrogenesis is based mainly on the transition elements, HFSEs, and REEs.

Although there are differences in the major element contents between the Diyanmiao gabbros and FABs, the compositional signatures of REEs, HFSEs, and large-ion lithophile elements (LILEs) are similar (Figure 5; Li et al., 2020a), suggesting a similar origin. The major-element compositions of the gabbros are similar to those of N-MORB, while the gabbros show a depleted REE pattern, indicating that their source more depleted than N-MORB source region. In comparison with N-MORB, the gabbros have variable enrichment in Rb, Ba, and K, and depletion in Nb, Ta, Zr, and Ti (Figure 5B), consistent with the characteristics of island-arc tholeiite in a subduction zone, suggesting the involvement of subduction fluids.

In a Th–Hf–Ta diagram, five gabbro samples plot in the N-MORB field, and two plots on or near the boundary between N-MORB and tholeiitic basalt (Figure 7A). In an Nb/Yb vs Th/Yb discrimination diagram, three gabbro samples plot within the weak subduction field, and four plots in the N-MORB field (Figure 7B). These results reveal a subduction-related signature for the gabbros. The gabbros also display a depletion trend relative to the estimated bulk mantle composition, as well as a Th enrichment trend in the volcanic arc field (Figure 7A), which is consistent with rock genetic models for the initial stages of the evolution of ensimatic marginal basins (Pearce et al., 1984). The Nb/La values of gabbro is 0.58–0.98 (mean=0.73), which is higher than the mean value of continental crust (Nb/La mean=0.7), but the crystallization differentiation does not lead to a decrease in Nb/La (Zhao et al., 1997). Therefore, the original magma of the Diyanmiao gabbro likely evolved by fluid metasomatism in an island-arc setting during oceanic subduction, rather than by crystallization and differentiation processes.

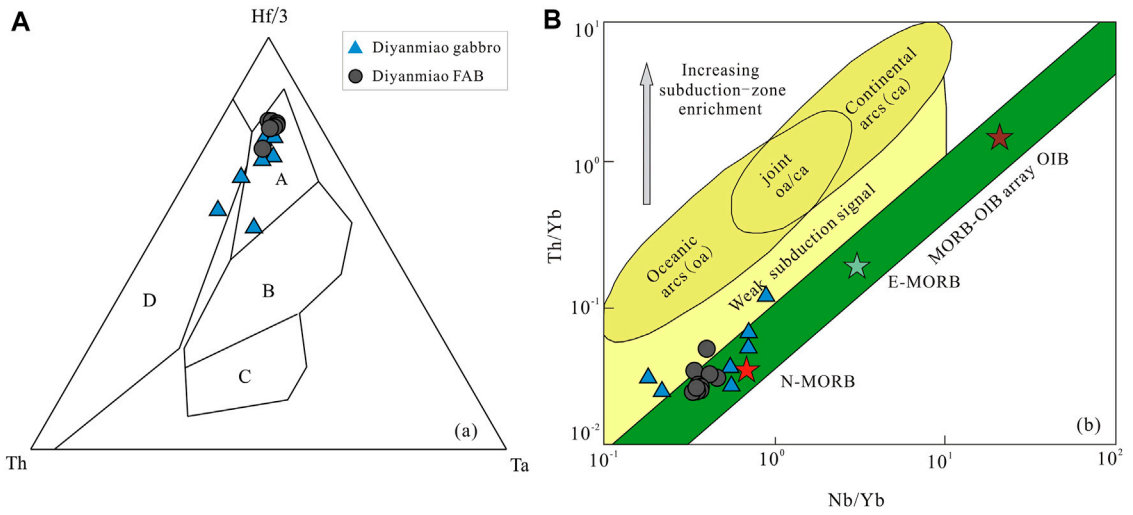

FIGURE 7
(A) Th-Hf-Ta diagram and **(B)** Th/Yb-Nb/Yb diagram for the gabbro and FAB in the Diyanmiao ophiolite. Data for FAB from Li et al., 2020a.

6.3 Tectonic implications of the gabbro: Constraints of intra-oceanic subduction in the southern Paleo-Asian ocean

The tectonic evolution of the CAOB is not yet fully resolved. This orogenic belt is thought to have formed by continuous accretion *via* multistage trench retreat or the simultaneous operation of multiple subduction zones (e.g., Xiao et al., 2009; Kröner et al., 2017). However, other studies have argued that the belt was formed by a series of orogenic processes involving collision, prolonged post-collisional stratification, and extension, with the PAO closing during the late Carboniferous–early Permian (e.g., Jahn et al., 2009; Han et al., 2011).

Uncertainty remains concerning the tectonic evolution of the EHOB, including the formation of the Hegenshan ophiolite, despite the efforts of many studies (e.g., Tang and Yan, 1993; Robinson et al., 1999; Xiao et al., 2003, 2009; Jian et al., 2008, 2010; Miao et al., 2008; Zhang et al., 2011; Eizenhöfer et al., 2014, 2015; Song et al., 2015). Some studies have proposed that the Hegenshan ophiolite formed in a mid-ocean-ridge environment (e.g., Nozaka and Liu, 2002; Song et al., 2015). Other studies have considered that the Hegenshan ophiolite formed in an SSZ environment, such as a back-arc tectonic environment (Miao et al., 2008; Wang et al., 2008; Eizenhöfer et al., 2014, 2015; Zhang et al., 2015) or an island arc–marginal basin system (Robinson et al., 1999).

The zircon U–Pb age of 294.4 ± 2.2 Ma obtained in this study for the Diyanmiao gabbro coincides with the formation age of late Carboniferous island-arc magmatic rocks in central Inner Mongolia that are found together with early Carboniferous Diyanmiao ophiolite (~340 Ma) (Li et al., 2018), forearc basalt (335.6 Ma), and boninite (~328 Ma) (Li et al., 2020a), and late Carboniferous adakite (315 Ma) (Wang et al., 2021). These results support the interpretation that the southern PAO had not closed by the early Permian but was undergoing intra-oceanic subduction. In other words, the late Carboniferous and early Permian ages record the initial stages of subduction of the Diyanmiao intra-oceanic arc within the southern PAO, with subsequent subduction of oceanic crust. On the basis of our field observations, geochemical data for the Diyanmiao ophiolite, and a comparison with the Izu–Bonin–Mariana initial subduction system (Ishizuka et al., 2014), we infer a model of subduction initiation in the Diyanmiao intra-oceanic arc during the early Carboniferous to early Permian. The initiation of early Carboniferous intra-oceanic subduction in the southeastern PAO began along a transform fault or fault zone (Li et al., 2020b) (Figure 8A). After the initial sinking of the slab, asthenospheric upwelling and decompression melting (Reagan et al., 2017) led to forearc spreading and the formation of the Diyanmiao FABs (335.6 Ma; Figure 8B; Li et al., 2020a; 2020b). As the subduction initiation process continued, leading to further decompression melting, boninites (328 Ma) were generated at this stage (Figure 8C). The newly discovered gabbro (294 Ma) may represent the magma event of the subducted plate at a greater depth (Figure 8D). The above information revealed that the initial subduction of intra-oceanic may have occurred in the eastern part of the Paleo-Asian Ocean from the early Carboniferous to the early Permian.

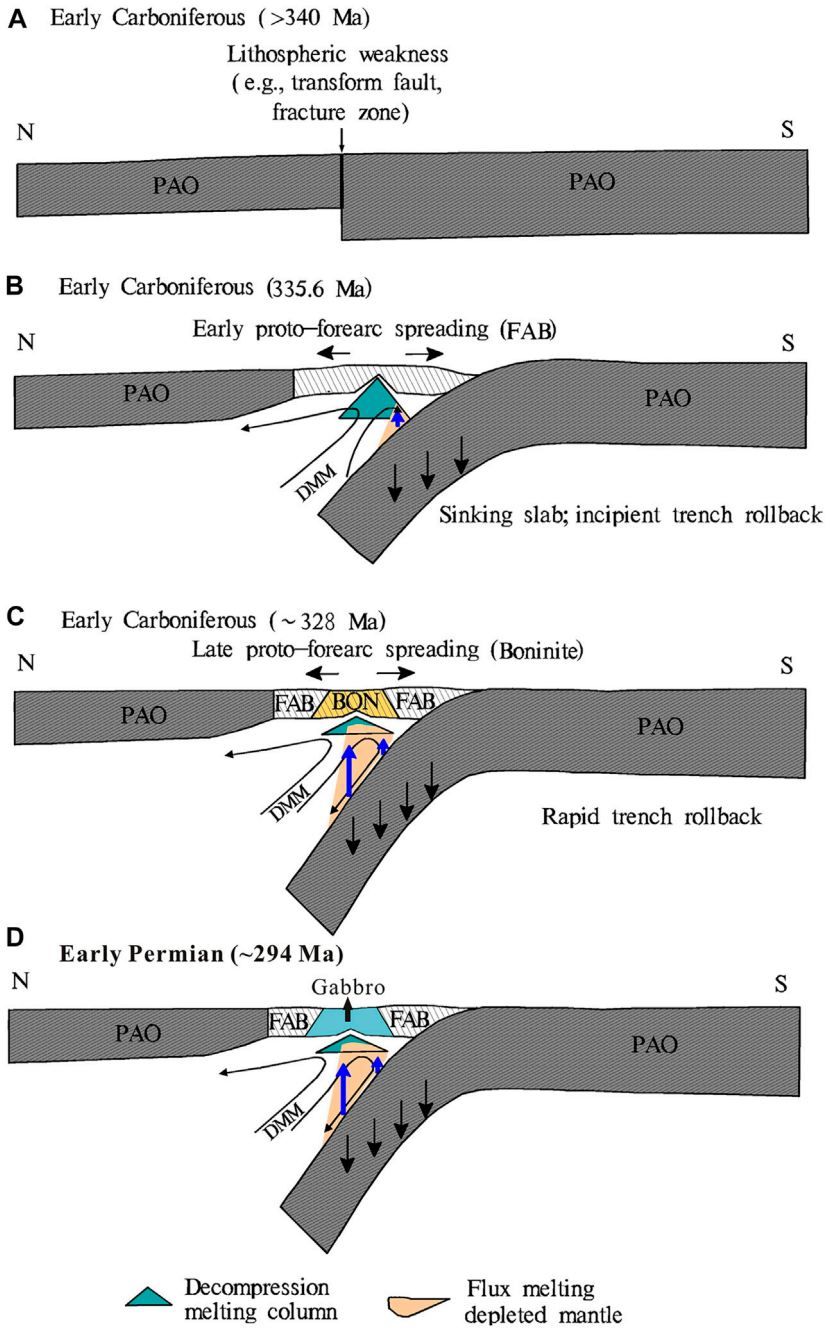

FIGURE 8
Evolution of the Early Carboniferous Diyanmiao intra-oceanic forearc system in the central Inner Mongolia, N China, as a typical example of subduction initiation of the southeastern PAO, based on the subduction infancy model (Whattam and Stern, 2011; Reagan et al., 2017). **(A)** Oceanic crust boundary preceding subduction initiation. **(B)** Early Carboniferous subduction initiation, leading to forearc spreading and formation of FABs. **(C)** As the subduction initiation process continued, boninites and transitional lavas were formed. **(D)** As the subduction process continued, the gabbro were formed. DMM is depleted MORB mantle.

The timing of the transformation of the PAO tectonic domain to the Paleo-Pacific tectonic domain has become an important Research Topic. Most studies have argued that the PAO tectonic system ended during the late Permian or Middle Triassic and continued locally through to the early Late Triassic (Xiao et al., 2003; Li, 2006; Wilde, 2015; Guo et al., 2016). Mao et al. (2020) proposed that late Permian to late Triassic igneous rocks on both sides of the Mongol–Okhotsk suture belt record an

active-continental-margin environment associated with bidirectional subduction of Mongol–Okhotsk oceanic lithosphere. Liang et al. (2021) argued that subduction of the Paleo-Pacific Plate began in the early Permian. Continued subduction triggered back-arc basin spreading during the early Permian–late Triassic (280–232 Ma). Closure of the basin resulted in the emplacement of accretionary materials in the Yuejinshan area during the late Triassic–early Jurassic (232–180 Ma), which also corresponds to the time of formation of high-pressure metamorphic belts on the southern margin of the Khanka Massif (230–220 Ma) and western margin of the Jiamusi Massif (210–180 Ma) (Zhou et al., 2014; Sun et al., 2015; Guo, 2016; Bi et al., 2017).

7 Conclusion

The geochemical characteristics of the Diyanmiao gabbro are similar to those of the Diyanmiao FABs. The gabbro is characterized by depletion in Nb, Ta, and Ti, similar to N-MORB, suggesting that the gabbro formed in a subduction setting in the Paleo-Asian Ocean. LA–MC–ICP–MS U–Pb dating of zircon grains from the Diyanmiao gabbro yielded an age of 294.4 ± 2.2 Ma, indicating that the gabbro from the Diyanmiao ophiolite formed during the early Permian. The initial subduction of intra-oceanic may have occurred in the eastern part of the Paleo-Asian Ocean from the early Carboniferous to the early Permian. Karimov et al., 2020, Shcherbakov et al., 2020, Xiao and Santosh, 2014.

Data availability statement

The original contributions presented in the study are included in the article/supplementary material, further inquiries can be directed to the corresponding author.

Author contributions

XZ: Investigation, Formal analysis, Visualization, Conceptualization, Supervision, Project administration, Funding acquisition, Writing—original draft, Writing—review & editing. YL: Supervision, Project administration, Funding acquisition. GW : Supervision, Project administration. SW: Project administration, Funding acquisition. XK: Project administration, Funding acquisition. XW: Project administration. ZL: Formal analysis, Funding acquisition.

Funding

This research was funded by the National Natural Science Foundation of China, Grant/Award Numbers: 41972061, China Geological Survey, Grant/Award Numbers: 1212011120711 and the Science and technology innovation team program of Hebei GEO University (KJCXTD-2021-07).

Conflict of interest

The authors declare that the research was conducted in the absence of any commercial or financial relationships that could be construed as a potential conflict of interest.

Publisher's note

References

Aldanmaz, E., Schmidt, M. W., Gourgaud, A., and Meisel, T. (2009). Mid-ocean ridge and supra-subduction geochemical signatures in spinel-peridotites from the neotethyan ophiolites in sw Turkey: Implications for upper mantle melting processes. *Lithos* 113 (3-4), 691–708. doi:10.1016/j.lithos.2009.03.010

Badarch, G., Gunningham, W. D., and Windley, B. F. (2002). A new terrane subdivision for Mongolia: Implications for the phanerozoic crustal growth of central asia. *J. Asian Earth Sci.* 21, 87–110. doi:10.1016/s1367-9120(02)00017-2

Bgmrimar (1996). Lithostratigraphy of the inner mongolia autonomous region. *Bureau of geology and mineral Resources of inner Mongolia autonomous region*, Wuhan: China University of Geosciences Press, 1–344. (in Chinese with English abstract).

Bi, J. H., Ge, W. C., Yang, H., Wang, Z. H., Tian, D. X., Liu, X. W., et al. (2017). Geochemistry of MORB and OIB in the yuejinshan complex, NE China: Implications for petrogenesis and tectonic setting. *J. Asian Earth Sci.* 145, 475–493. doi:10.1016/j.jseaes.2017.06.025

Boynton, W. V. (1984). "Cosmochemistry of the rare earth elements: Meteorite studies," in *Rare earth element geochemistry. Developments in geochemistry*. Editor P. E. Henderson (Amsterdam: Elsevier), 63–114.

Chen, B., Jahn, B. M., and Tian, W. (2009). Evolution of the solonker suture zone: Constraints from zircon U-Pb ages, Hf isotopic ratios and whole-rock Nd-Sr isotope compositions of subduction-and collision-related magmas and forearc sediments. *J. Asian Earth Sci.* 34, 245–257. doi:10.1016/j.jseaes.2008.05.007

Cheng, Y. H., Duan, L. F., Wang, S. Y., Li, Y., Teng, X. J., and Zhang, T. F. (2019). Termination of the hegenshan orogen in the xing'an-Mongolian orogenic belt, north China: Geochemical and zircon U-Pb geochronological constraints from early permian mafic dykes. *Geol. J.* 55 (1), 845–861. doi:10.1002/gj.3463

Cheng, Y. H., Li, M., Zhang, T. F., Li, Y. F., Li, Y., Niu, W. C., et al. (2015). Late Paleozoic crustal extensional regime on the Southeastern Siberian Plate:new evidences from geochronology and geochemistry of the bojite in the Dong Ujimqi. *Acta Geol. Sin.* 89 (2), 262–271. (in Chinese with English abstract).

Cheng, Y. H., Teng, X. J., Li, Y. F., Li, M., and Zhang, T. F. (2014). Early permian east-ujimqin mafic–ultramafic and granitic rocks from the xing'an–Mongolian orogenic belt, north China: Origin, chronology, and tectonic implications. *JAES* 96, 361–373. doi:10.1016/j.jseaes.2014.09.027

Dilek, Y., and Furnes, H. (2011). Ophiolite Genesis and global tectonics: Geochemical and tectonic fingerprinting of ancient oceanic lithosphere. *Geol. Soc. Am. Bull.* 123, 387–411. doi:10.1130/b30446.1

Dilek, Y., and Furnes, H. (2014). Ophiolites and their origins. *Elements* 10, 93–100. doi:10.2113/gselements.10.2.93

Dilek, Y., and Furnes, H. (2009). Structure and geochemistry of Tethyan ophiolites and their petrogenesis in subduction rollback systems. *Lithos* 113, 1–20. doi:10.1016/j.lithos.2009.04.022

Dilek, Y., and Robinson, P. T. (2003). Ophiolites in Earth history: Introduction. *Geol. Soc. Lond. Special Publ.* 218 (1), 1–8. doi:10.1144/gsl.sp.2003.218.01.01

Dobretsov, N. L., Berzin, N. A., and Buslov, M. M. (1995). Opening and tectonic evolution of the paleo-Asian ocean. *Int. Geol. Rev.* 37, 335–360. doi:10.1080/00206819509465407

Eizenhöfer, P. R., Zhao, G., Sun, M., Zhang, J., Han, Y. G., and Hou, W. (2015). Geochronological and Hf isotopic variability of detrital zircons in Paleozoic strata across the accretionary collision zone between the North China craton and Mongolian arcs and tectonic implications. *Geol. Soc. Am. Bull.* 127, 1422–1436. doi:10.1130/b31175.1

Eizenhöfer, P. R., Zhao, G., Zhang, J., and Sun, M. (2014). Final closure of the paleo-Asian ocean along the solonker suture zone: Constraints from geochronological and geochemical data of permian volcanic and sedimentary rocks. *Tectonics* 33, 441–463. doi:10.1002/2013tc003357

Ge, M. C., Zhou, W. X., Yu, Y., Sun, J. J., Bao, J. Q., and Wang, S. H. (2011). Dissolution and supracrustal rocks dating of Xilin Gol complex, Inner Mongolia, China. *Earth Sci. Front.* 18 (5), 182–195.

Gillis, K. M., and Banerjee, N. R. (2000). "Hydrothermal alteration patterns in supra-subduction zone ophiolites," in *Special Paper of the Geological Society of America*. 349, Editors Y. Dilek and E. M. Moores, 283–297.

Guo, Y. (2016). *The nature of yuejinshan complex in the eastern part of heilongjiang Province and its evolution PhD thesis*. Jilin University. Changchun, China, (in Chinese with English abstract).

Han, B. F., He, G. Q., Wang, X. C., and Guo, Z. J. (2011). Late carboniferous collision between the Tarim and Kazakhstan-yili terranes in the Western segment of the south tian Shan orogen, central asia, and implications for the northern xinjiang, Western China. *Earth Sci. Rev.* 109, 74–93. doi:10.1016/j.earscirev.2011.09.001

Ishizuka, O., Tani, K., and Reagan, M. K. (2014). Izu-Bonin-Mariana forearc crust as a modern ophiolite analogue. *Elements* 10, 115–120. doi:10.2113/gselements.10.2.115

Jahn, B. M. (2004). The Central Asian Orogenic Belt and growth of the continental crust in the Phanerozoic. *Geological Society of London, Special Publication*, 226, 73–100, doi:10.1144/GSL.SP.2004.226.01.05

Jahn, B. M., Litvinovsky, B. A., Zanvilevich, A. N., and Reichow, M. (2009). Peralkaline granitoid magmatism in the Mongolian–Transbaikalian Belt: Evolution, petrogenesis and tectonic significance. *Lithos* 113, 521–539. doi:10.1016/j.lithos.2009.06.015

Jian, P., KrÖner, A., Windley, B. F., Shi, Y. R., Zhang, W., Zhang, L. Q., et al. (2012). Carboniferous and cretaceous mafic–ultramafic massifs in inner Mongolia (China): A SHRIMP zircon and geochemical study of the previously presumed integral "hegenshan ophiolite". *Lithos* 142 (143), 48–66. doi:10.1016/j.lithos.2012.03.007

Jian, P., Liu, D., KrÖner, A., Windley, B. F., Shi, Y., Zhang, F., et al. (2008). Time scale of an early to mid-paleozoic orogenic cycle of the long-lived central asian orogenic belt, inner Mongolia of China: Implications for continental growth. *Lithos* 101, 233–259. doi:10.1016/j.lithos.2007.07.005

Jian, P., Liu, D., Kroner, A., Windley, B. F., Shi, Y., Zhang, W., et al. (2010). Evolution of a permian intraoceanic arc-trench system in the solonker suture zone, central asian orogenic belt, China and Mongolia. *Lithos* 118, 169–190. doi:10.1016/j.lithos.2010.04.014

Karimov, A. A., Gornova, M. A., Belyaev, V. A., Ya Medvedev, A., V Bryanskiy, N., and V. Bryanskiy, N. (2020). Genesis of pyroxenite veins in supra-subduction zone peridotites: Evidence from petrography and mineral composition of Egiingol massif (Northern Mongolia). *China Geol.* 3, 299–313. doi:10.31035/cg2020035

Kröner, A., Kovach, V., Aledeiev, D., Wang, K. L., Wong, J., Degtyarev, K., et al. (2017). No excessive crustal growth in the central asian orogenic belt: Further evidence from field relationships and isotopic data. *Gondwana Res.* 50, 135–166. doi:10.1016/j.gr.2017.04.006

Kusky, T. M. (2011). Geophysical and geological tests of tectonic models of the North China Craton. *Gondwana Res.* 20 (1), 26–35. doi:10.1016/j.gr.2011.01.004

Li, J. Y. (2006). Permian geodynamic setting of northeast China and adjacent regions: Closure of the paleo-Asian ocean and subduction of the Paleo-Pacific Plate. *J. Asian Earth Sci.* 26, 207–224. doi:10.1016/j.jseaes.2005.09.001

Li, K., Zhang, Z. C., Feng, Z. S., Li, J. F., Tang, W. H., and Luo, Z. W. (2014). Zircon SHRIMP U-Pb dating and its geological significance of the Late-Carboniferous to Early-Permian volcanic rocks in Bayanwula area, the central of Inner Mongolia. *Acta Petrol. Sin.* 30 (7). (in press)(in Chinese with English abstract).

Li, Y. J., Wang, G. H., Santosh, M., Wang, J. F., Dong, P. P., and Li, H. Y. (2020a). Subduction initiation of the SE paleo-Asian ocean: Evidence from a well preserved intra-oceanic forearc ophiolite fragment in central inner Mongolia, north China. *Earth Planet. Sci. Lett.* 535 (1), 116087doi:10.1016/j.epsl.2020.116087

Li, Y. J., Wang, G. H., Santosh, M., Wang, J. F., Dong, P. P., and Li, H. Y. (2018). Supra-subduction zone ophiolites from inner Mongolia, north China: Implications for the tectonic history of the southeastern central asian orogenic belt. *Gondwana Res.* 59, 126–143. doi:10.1016/j.gr.2018.02.018

Li, Y. J., Wang, J. F., Li, H. Y., and Dong, P. P. (2015). Recognition of meilaotewula ophiolite in xi Ujimqin banner, inner Mongolia. *Acta Petrol. Sin.* 31 (5), 1461–1470. (in Chinese with English abstract).

Li, Y. J., Wang, J. F., Xin, H. T., and Dong, P. P. (2020b). Subduction initiation in the southeastern Palaeo-Asian Ocean: Constraints from early Permian adakites in suprasubduction zone ophiolites, central Inner Mongolia, North China. *Geol. J.* 55, 2044–2061. doi:10.1002/gj.3696

Liang, R. (1991). "The characteristics of the ophiolite sequences and its rock associations in central and eastern Inner Mongolia," in *Pre-jurassic geology of inner Mongolia, China*. Editors K. Ishii, X. Liu, K. Ichikawa, and B. Huang (Osaka: China-Japan Cooperative Research Group), 65–84.

Liang, Y., Zheng, H., Li, H., Algeo, T., and Sun, X. M. (2021). Late paleozoic–mesozoic subduction and accretion of the Paleo-Pacific Plate: Insights from ophiolitic rocks in the wandashan accretionary complex, NE China. *Geosci. Front.* 12 (6), 101242doi:10.1016/j.gsf.2021.101242

Liu, Y. S., Hu, Z. C., Gao, S., Detlef, G., Xu, J., Gao, C. G., et al. (2008). *In situ* analysis of major and trace elements of anhydrous minerals by LA–ICP–MS without applying an internal standard. *Chem. Geol.* 257 (1–2), 34–43. doi:10.1016/j.chemgeo.2008.08.004

Ludwig, K. R. (2003). *User's manual for isoplot 3.00: A geochronological toolkit for microsoft excel*, 4. Berkeley: Special Publication Geochronology Center, 1–70.

Ma, Y. F., Liu, Y. J., Peskov, A., Wang, Y., Song, W. M., Zhang, Y. J., et al. (2021). Paleozoic tectonic evolution of the eastern central asian orogenic belt in NE China, *China geology*, 5.

Mao, A. Q., Sun, D. Y., Gou, J., Yang, D. G., and Zheng, H. (2020). Late palaeozoic–early mesozoic southward subduction of the mongol–okhotsk oceanic slab: Geochronological, geochemical, and Hf isotopic evidence from intrusive rocks in the erguna massif (NE China). *Int. Geol. Rev.* 63 (10), 1262–1287. doi:10.1080/00206814.2020.1758968

Miao, L. C., Zhang, F. Q., Fan, W. M., and Liu, D. Y. (2007). Phanerozoic evolution of the Inner Mongolia-Daxinganling orogenic belt in North China: constraints from geochronology of ophiolites and associated formations, *Geological Society of London, Special Publication*, 280, 223–237.

Miao, L. C., Fan, W. M., Liu, D. Y., Zhang, F. Q., Shi, Y. R., and Guo, F. (2008). Geochronology and geochemistry of the hegenshan ophiolitic complex: Implications for late-stage tectonic evolution of the inner Mongolia-daxinganling orogenic belt, China. *J. Asian Earth Sci.* 32 (5–6), 348–370. doi:10.1016/j.jseaes.2007.11.005

Nicolas, A. (1989). *Structures of ophiolites and dynamics of oceanic lithosphere*. Kluwer Academic Publishers, New York, MA, UK, 367.

Nozaka, T., and Liu, Y. (2002). Petrology of the Hegenshan ophiolite and its implication for the tectonic evolution of northern China. *Earth Planet. Sci. Lett.* 202, 89–104. doi:10.1016/s0012-821x(02)00774-4

Osozawa, S., Shinjo, R., Lo, C. H., Jahn, B. M., Hoang, N., Sasaki, M., et al. (2012). Geochemistry and geochronology of the Troodos ophiolite: An SSZ ophiolite generated by subduction initiation and an extended episode of ridge subduction? *Lithosphere* 4, 497–510. doi:10.1130/l205.1

Pearce, J. A. (1983). "The role of sub-continental lithosphere in magma Genesis at destructive plate margins. et al," in *Continental basalts and mantle xenoliths*. Editor Hawkesworth Cheshire, England, (Nantwich Shiva), 230–249.

Pearce, J. A. (2008). Geochemical fingerprinting of oceanic basalts with applications to ophiolite classification and the search for Archean oceanic crust. *Lithos* 100, 14–48. doi:10.1016/j.lithos.2007.06.016

Pearce, J. A., Lippard, S. J., and Roberts, S. (1984). Characteristics and tectonic significance of supra-subduction zone ophiolites. *Geol. Soc. Lond. Spec. Publ.* 16, 77–94. doi:10.1144/gsl.sp.1984.016.01.06

Reagan, M. K., Pearce, J. A., Petronotis, K., Almeev, R., Avery, A. J., Carvallo, C., et al. (2017). Subduction initiation and ophiolite crust: New insights from IODP drilling. *Int. Geol. Rev.* 59, 1439–1450. doi:10.1080/00206814.2016.1276482

Robinson, P. T., Zhou, M. F., Hu, X. F., Reynolds, P., Bai, W. J., and Yang, J. (1999). Geochemical constraints on the origin of the Hegenshan ophiolite, Inner Mongolia, China. *J. Asian Earth Sci.* 17, 423–442. doi:10.1016/s1367-9120(99)00016-4

Safonova, I. (2017). Juvenile versus recycled crust in the central asian orogenic belt: Implications from ocean plate stratigraphy, blueschist belts and intra-oceanic arcs. *Gondwana Res.* 47, 6–27. doi:10.1016/j.gr.2016.09.003

Santosh, M., Hu, C. N., He, X. F., Li, S. S., Tsunogae, T., Shaji, E., et al. (2017). Neoproterozoic arc magmatism in the southern madurai block, India: Subduction, relamination, continental outbuilding, and the growth of gondwana. *Gondwana Res.* 45, 1–42. doi:10.1016/j.gr.2016.12.009

Santosh, M., Teng, X. M., He, X. F., Tang, L., and Yang, Q. Y. (2016). Discovery of neoarchean suprasubduction zone ophiolite suite from yishui complex in the north China craton. *Gondwana Res.* 38, 1–27. doi:10.1016/j.gr.2015.10.017

Shcherbakov, Y. D., Perepelov, A. B., and Svetlana Tsypukova, S. (2020). Report on Late Paleozoic bimodal volcanic associations discovered in Northern Mongolian Rift zone. *China Geol.* 3, 496–500.

Shervais, J. W., Kimbrough, D. L., Renne, P., Murchey, B., Snow, C. A., Schaman, R. M. Z., et al. (2004). Multi-stage origin of the coast range ophiolite, California: Implications for the life cycle of supra-subduction zone ophiolites. *Int. Geol. Rev.* 46, 289–315. doi:10.2747/0020-6814.46.4.289

Shervais, J. W. (2001). Birth, death, and resurrection: The life cycle of suprasubduction zone ophiolites. *Geochem. Geophys. Geosystems* 2. doi:10.1029/2000gc000080

Song, S. G., Wang, M. M., Xu, X., Wang, C., Niu, Y., Allen, M. B., et al. (2015). Ophiolites in the xing'an-inner Mongolia accretionary belt of the CAOB: Implications for two cycles of seafloor spreading and accretionary orogenic events. *Tectonics* 34, 2221–2248. doi:10.1002/2015tc003948

Sun, L. X., Ren, B. F., Zhao, F. Q., Gu, Y. C., Li, Y. C., and Liu, H. (2013). Zircon U–Pb dating and Hf isotopic compositions of the Mesoporterozoic granitic gneiss in Xilinhot Block, Inner Mongolia. *Geol. Bull. China* 32, 327–340. (in Chinese with English abstract).

Sun, M. D., Xu, Y. G., Wilde, S. A., Chen, H. L., and Yang, S. F. (2015). The permian dongfanghong island-arc gabbro of the wandashan orogen, NE China: Implications for paleo-pacific subduction. *Tectonophys* 659, 122–136. doi:10.1016/j.tecto.2015.07.034

Sun, S. S., and McDonough, W. F. (1989). *Chemical and isotopic systematics of oceanic basalts: implications for mantle composition and processes,. Geological Society of London, Special Publication*, 42, 313–340.

Tang, K. D. (1990). Tectonic development of Paleozoic foldbelts at the north margin of the Sino-Korean Craton. *Tectonics* 9, 249–260. doi:10.1029/tc009i002p00249

Tang, K., and Yan, Z. (1993). Regional metamorphism and tectonic evolution of the Inner, *J. Metamorph. Geol.*, 11, 511–522.

Wang, Q., and Liu, X. Y. (1986). Paleoplate tectonics between cathaysia and angaral and in inner Mongolia of China. *Tectonics* 5, 1073–1088. doi:10.1029/tc005i007p01073

Wang, S., Li, Y. J., Wang, J. F., Dong, P. P., Li, H. Y., Guo, L. L., et al. (2021). Discovery of late carboniferous adakite in manita, inner Mongolia, and its constrains on intra-oceanic subduction in eastern paleo-Asian ocean. *Geol. Bull. China* 40, 82–94. (In Chinese with English Abstract).

Wang, S. Q., Xu, J. F., Liu, X. J., and Hou, Q. Y. (2008). Geochemistry of the chaokeshan ophiolite: Product of intra-oceanic back-arc basin? *Acta Petrol. Sin.* 24, 2869–2879. (in Chinese with English abstract).

Whattam, S. A., and Stern, R. J. (2011). The'subduction initiation rule': A key for linking ophiolites, intra-oceanic forearcs, and subduction initiation. *Contrib. Mineral. Pet.* 162, 1031–1045. doi:10.1007/s00410-011-0638-z

Wilde, S. A. (2015). Final amalgamation of the central asian orogenic belt in ne China: Paleo-Asian ocean closure versus Paleo-Pacific Plate subduction — a review of the evidence. *Tectonophysics* 662, 345–362. doi:10.1016/j.tecto.2015.05.006

Windley, B. F., Alexeiev, D., Xiao, W. L., KrÖner, A., and Badarch, G. (2007)., 164. London, 31–47. doi:10.1144/0016-76492006-022Tectonic models for accretion of the central asian orogenic belt*J. Geol. Soc.*

Windley, B. F., and Allen, M. B. (1993). Mongolian plateau: Evidence for a late cenozoic mantle plume under central Asia. *Geology* 21 (4), 295–298. doi:10.1130/0091-7613(1993)021<0295:mpefal>2.3.co;2

Xiao, W. J., and Santosh, M. (2014). The Western central asian orogenic belt: A window to accretionary orogenesis and continental growth. *Gondwana Res.* 25, 1429–1444. doi:10.1016/j.gr.2014.01.008

Xiao, W. J., Windley, B. F., Hao, J., and Zhai, M. G. (2003). Accretion leading to collision and the permian solonker suture, inner Mongolia, China: Termination of the central asian orogenic belt. *Tectonics* 22 (1069). doi:10.1029/2002tc001484

Xiao, W. J., Windley, B. F., Yuan, C., Sun, M., Han, C. M., Lin, S. F., et al. (2009). Paleozoic multiple subduction-accretion processes of the southern Altaids. *Am. J. Sci.* 309, 221–270. doi:10.2475/03.2009.02

Xu, B., Charvet, J., Chen, Y., Zhao, P., and Shi, G. (2013). Middle Paleozoic convergent orogenic belts in Western Inner Mongolia (China): Framework, kinematics, geochronology and implications for tectonic evolution of the Central Asian Orogenic Belt. *Gondwana Res.* 23 (4), 1342–1364. doi:10.1016/j.gr.2012.05.015

Yang, F., Kim, S. W., Tsunogae, T., and Zhou, H. (2021). Multiple enrichment of subcontinental lithospheric mantle with Archean to Mesozoic components: Evidence from the Chicheng ultramafic complex, North China Craton. *Gondwana Res.* 94, 201–221.

Yang, F., Santosh, M., Tsunogae, T., Tang, L., and Teng, X. (2017). Multiple magmatism in an evolving suprasubduction zone mantle wedge: the case of the composite mafic-ultramafic complex of Gaositai, North China Craton. *Lithos* 284, 525–544.

Zhang, X. H., Wilde, S. A., Zhang, H. F., and Zhai, M. G. (2011). Early permian high-K calc-alkaline volcanic rocks from NW inner Mongolia, north China: Geochemistry, origin and tectonic implications. *J. Geol.Soc* 168, 525–543. doi:10.1144/0016-76492010-094

Zhang, Z. C., Li, K., Li, J. F., Tang, W. H., Chen, Y., and Luo, Z. W. (2015). Geochronology and geochemistry of the eastern Erenhot ophiolitic complex: Implications for the tectonic evolution of the inner Mongolia–daxinganling orogenic belt. *J. Asian Earth Sci.* 97, 279–293. doi:10.1016/j.jseaes.2014.06.008

Zhao, P., Faure, M., Chen, Y., Shi, G. Z., and Xu, B. (2015). A new Triassic shortening-extrusion tectonic model for Central-Eastern Asia: Structural, geochronological and paleomagnetic investigations in the Xilamulun Fault (North China). *Earth Planet. Sci. Lett.* 426, 46–57. doi:10.1016/j.epsl.2015.06.011

Zhao, Z. H., and Zhou, L. D. (1997). REE geochemistry of some alkali-rich intrusive rocks in China. *Sci. China Ser. D* 40 (2), 145–158. doi:10.1007/bf02878373

Zhou, J. B., Cao, J. L., Wilde, S. A., Zhao, G. C., Zhang, J. J., and Wang, B. (2014). Paleo-Pacific subduction-accretion: Evidence from Geochemical and U-Pb zircon dating of the Nadanhada accretionary complex, NE China. *Tectonics* 33 (12), 2444–2466. doi:10.1002/2014tc003637